Gamma-Induced Image Degradation Analysis of Robot Vision Sensor for Autonomous Inspection of Nuclear Sites

Zeba Khanam, Bilal Aslam, Sangeet Saha, Xiaojun Zhai, *Member, IEEE*, Shoaib Ehsan, *Senior Member, IEEE*, Rustam Stolkin, *Member, IEEE*, and Klaus McDonald-Maier, *Senior Member, IEEE*

***Abstract*—There is an increasing desire to conduct autonomous inspection of nuclear sites using robots. However, the presence of gamma radiation in nuclear sites induces degradation in vision sensors. In this paper, the effects of gamma radiation on a robot vision sensor (CMOS camera) used for radiological inspection is examined. The analyses have been carried out for two types of images at different dose rates: a) dark images b) illuminated images. In this work, dark images and chessboard images under illumination are analysed using various evaluation metrics to evaluate the effect of gamma radiation on CMOS Integrated Circuit (IC) and electronic circuitry of the sensor. Experimental results manifest significant changes in electrical properties like the generation of radiation-induced photo signal in sensing circuitry and radiation-induced noise affecting the visual odometry of the robot. System-level degradation for gamma dose rates upto 3 Gy/min intensifies, making data from the imaging sensor unreliable for the visual odometry. However, images captured for gamma dose rate upto 3 Gy/min can be used for surveillance purpose.**

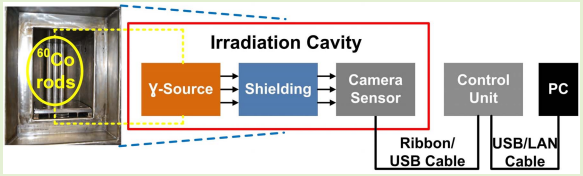

***Index Terms*—Gamma-induced image degradation, CMOS image sensor, robotic inspection, vision sensor degradation.**

I. Introduction

SINCE the inception of commercial nuclear sites, robots have played a crucial role due to their ability to access hazardous areas [1]. However, the catastrophic Fukushima-Daiichi accident has created a global demand to deploy the robots for periodic inspection of nuclear sites. Tele-operated robots like JAEA-3 and Quinc have conducted inspection of Fukushima facility in the past [2]. A recent attempt of radiological monitoring of Sellafield, the largest nuclear site in Europe, using an autonomous robot has been made [3]. The inspection of nuclear site is a cumbersome and challenging task which requires robots to be equipped with CMOS image sensors to perform real-time tasks like visual odometry and calibration.

However, the grave challenges of autonomous inspection using vision sensors are intensified for nuclear facilities by the presence of radioactive elements. These elements can trigger degradation of sensors at a rapid rate and resulting in complete breakdown of the robot inside the site [4]. The vulnerability of CMOS image sensors to radioactive elements stems from the fact that the CMOS Integrated Circuit (IC) of the sensor which consists of a pixel array, address decoders and signal processing circuit is exposed to the precarious environment. Extensive research has been done to evaluate the effects of radiation on semiconductor devices [5]–[8], range finding devices [9], [10] and acoustic sensors [11]. The evaluation of the effect of radiation on CMOS image sensors has focused on sensor built using radiation-hardened design [12].

The performance of cameras built using commercially available radiation-hardened CMOS image sensors have been

Manuscript received 7 November 2020; revised 5 January 2021; accepted 5 January 2021. Date of publication 8 January 2021; date of current version 14 September 2022. This work was supported by the U.K. Engineering and Physical Sciences Research Council under Grant EP/R02572X/1 and Grant EP/P017487/1. The associate editor coordinating the review of this article and approving it for publication was Dr. Yin Zhang. *(Zeba Khanam and Bilal Aslam contributed equally to this work.) (Corresponding author: Zeba Khanam.)*

Zeba Khanam, Bilal Aslam, Sangeet Saha, Xiaojun Zhai, Shoaib Ehsan, and Klaus McDonald-Maier are with the Embedded and Intelligent Systems Laboratory, University of Essex, Colchester CO4 3SQ, U.K. (e-mail: zeba.khanam@essex.ac.uk; ba18997@essex.ac.uk; sangeet.saha@essex.ac.uk; xzhai@essex.ac.uk; sehsan@essex.ac.uk; kdm@essex.ac.uk).

Rustam Stolkin is with the Extreme Robotics Laboratory (ERL), University of Birmingham, Birmingham B15 2TT, U.K. (e-mail: r.stolkin@cs.bham.ac.uk).

Digital Object Identifier 10.1109/JSEN.2021.3050168

evaluated under various dose rates [13], [14]. The evaluation of effects of gamma rays on industrial camera based on CMOS image sensors has been conducted in recent past [15]. Another research work has focused on measuring the gamma-induced image degradation using Commercial Off-The-Shelf (COTS) image sensor [16]. Recent works have analysed a fixed pattern, temporal noise degradation and total ionizing dose induced by gamma rays, protons and neutrons in pinned photodiode CMOS image sensors [17]–[19] giving a new direction to the research. In some recent works, the COTS CMOS image sensors have been used as gamma ray detector [20], [21]. Goiffon et. al [22] had discovered several original radiation effects such as an increase in pinning voltage, decrease in buried photodiode well capacity to name a few, when pinned photodiode CMOS Image sensor was exposed to 10 KGy ionizing radiation. Another study [23] showed that radiation exposure damages the gain brought by the epitaxial layer thickness in pinned photo diode CMOS image sensors.

Recent advancement in imaging technologies has led to deployment of the COTS CMOS cameras for robots due to their low cost and weight, compact size, ease of use and compact data storage [3], [24]. With the deployment of robots to inspect nuclear sites, there exists a research gap where image degradation analysis of COTS CMOS image sensors used as a robot vision sensor needs to be conducted. In this work, we aim to bridge this research gap by analysing the degradation in dark images and images captured in illumination when the Raspberry Pi camera (a robot vision camera) is exposed to different dose rates of gamma radiation.

To this end, we had investigated the performance of three such COTS CMOS image sensors under gamma radiation exposure [25]. The three sensors analysed were: 1) Raspberry Pi camera [26], 2) Spy Camera [27] and 3) Trust USB Camera [28]. The experimental evaluation pointed out that the image degradation was less in Rapberry Pi camera as compared to other two. The reason behind better performance of Rapberry Pi camera can be attributed to the smaller pixel sensitive volume which in turn generates less gamma-induced photo signal allowing better performance. Taking a step further in this work, we measure the degradation in the images captured by Raspberry Pi camera during exposure of gamma radiation in detail. The main motivation behind this study is that the Raspberry Pi camera has been used as a robot vision sensor in the CARMA robot which had recently successfully monitored Sellafield nuclear site [3].

The radiation environment of any nuclear site consists of a mixture of α, β, γ and neutron emitters [29]–[31]. Gamma rays are of particular concern due to their high penetration power, occurrence in nuclear decay chains and high dose rates. This is the main reason that majority of robots deployed for inspection of the nuclear facilities have focused on γ radiation [32]. In this paper, we study the degradation of Raspberry Pi sensor due to gamma radiation in two different directions by calculating various evaluation metrics. The first direction deals with the effect of radiation in dark conditions and second direction deals with the effect of radiation on captured images in presence of light source. Both these directions illustrate the effect of gamma radiation on the physical element of the sensor and electronic circuitry. Furthermore, a study has been carried out to elucidate the difference between the effects of gamma flux and received cumulative dose on the Raspberry Pi camera during the radiation exposure. A pertinent effort has been made to investigate the impact of gamma radiation when the sensor is still operational. Furthermore, a study has been carried out to elucidate the difference between the effects of the dose rate and the evolution of evaluation metrics with time on the Raspberry Pi camera.

The remainder of the paper is organised as follows. Section II provides an overview of the background studies in this area. This is followed by a discussion on experimental realisation in Section III. The analysis of dark images is presented in-detail in Section IV. In Section V, we analyse the images captured in presence of light source. The conclusion of the investigative study is presented in Section VI.

II. Background Studies

A nuclear environment exhibits several characteristics like a variable radiation field, unstructured and potentially unpredictable physical environments, extreme environmental conditions (high temperature, pressure, steam, dust, non-homogeneous illumination) and limited communication bandwidth. These characteristics pose significant challenges to sensors, especially, to CMOS image sensor which assists robot to interpret its environment.

A. Robotic Inspection of Nuclear Sites

The history of the deployment of ground-based robots for radiological inspection resonates with the occurrence of three major nuclear accidents: *1)Three Mile, 2) Chernobyl and 3) Fukushima Daiichi*. The need for inspection of nuclear site became an imperative, after first nuclear power plant disaster of Three Mile in 1979. This resulted in deployment of the first ever radiation survey robots like ROVER, LOUIE I and LOUIEE II, which were remotely-operated in the basement of nuclear facility after four years following the accident [24]. Even though these robots had their own limitations centering around autonomous navigation and failure recovery, they are still lauded as a landmark in the nuclear industry.

Seven years later, the catastrophic accident of Chernobyl initiated the immediate response in the form of deployment of two tele-operated robots (STR-1). However, sensors deployed in both the robots were rapidly disabled by the presence of radioactive substances [33]. Since then, steadfast technological advances have resulted in the development of sophisticated robots with latest sensors which have successfully made inroads into fields like transportation, industry and medicine. However, the Fukushima accident in 2011 demonstrated that our current robots have not reached required standard of deployment in such extreme environments.

The robotics community dealt with this setback by modifying many robots and making them tailor-made for radiation inspection like JAEA-3 and Quince [2]. These tele-operated robots infused confidence in research industry and saw a series of robots like RICA [Robot d'Inspection pour Cellules Aveugles] [34] and co-robots developed by Georgia Institute of Technology [35] performing radiation survey with the help of human input.

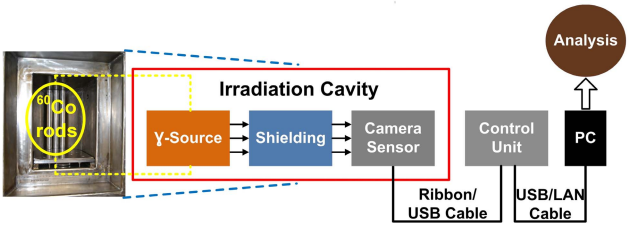

Fig. 1. Experimental Setup at DCF, UK.

However, the Fukushima Daiichi accident unveiled the specific requirement which robotic technology needs to meet for deployment of robots in nuclear facility. The main requirement was autonomous inspection of site in minimum time using machine vision sensors. A major milestone to meet this requirement was the development of CARMA (Continuous Autonomous Radiation-Monitoring Assistance) [3] in 2018 for autonomous radiation inspection of Sellafield, the largest nuclear site of Europe.

B. Effects of Gamma Radiation on Robot Vision Sensors

Robot vision sensors, CMOS devices, are an integral part of image capturing subsystem of robot. Gamma ray induces total ionising dose which affects CMOS and semiconductor electronic materials as well as a variety of other materials used in the robot [32]. A particle radiation incident on any semiconductor surface deposits energy which creates electron-hole pairs in the semiconductor. The most notable effects occur in insulator in the semiconductor like gate or field oxides in CMOS devices. In the electron-hole pair, the low mobility of holes allows them to exit the insulator, slowly as compared to electrons. With passage of time and accumulated dose, this behaviour of holes allows positive charge to build up.

The oxide trapped charges invoke a series of changes in the electrical property of the sensors, for instance generation of increased leakage current in CMOS transistor. COTS robot vision sensors along with lenses contain signal processing electronics, communication ports and voltage regulation. The Raspberry Pi camera is an excellent choice for robot vision sensors used in radiological inspection as it contains minimal signal processing circuitry, making it less vulnerable to change in electrical characteristics [25]. The effect of gamma radiation on Raspberry Pi sensors is a combination of the radiation effects on the CMOS IC and electronic circuitry. Field reports from Fukushima Daiichi nuclear facility have shown the presence of gamma radiations with dose rate upto 6.5 rad/hour (0.0011 Gy/min), with the anticipation of higher dose rates near the reactor [36]. According to the measurements performed in 2017 at the crippled Fukushima Power Plant, the gamma dose rate in the contaminated vessel of the reactor were close to 9 Gy/min [37]. The studies [38], [39] conducted at the Chernobyl nuclear site provide an approximate measured radiation levels in the vicinity of the main damaged reactor of the Chernobyl Nuclear Power Plant immediately after the accident. The gamma dose rate were as high as 5 Gy/min close to the reactor core, and fell to 2.5 mGy/min in the nearby concrete mixing unit.

Therefore, we analyse the degradation upto 4 Gy/min under two circumstances: dark images and light images. The dark images allow us to calculate metrics like the gamma-induced photo signal which is the leakage current reflecting the leakage mechanism occurring in the sensing element. The radiation effect is analysed for images captured in presence of light source by evaluating the image quality and handcrafted features reflecting the changes induced in sensing element and electronic circuitry by gamma radiation.

III. Experimental Realization

A. Experimental Setup

1) Dalton Cumbrian Facility (DCF): A $Co-60$ self shielded irradiator located at the DCF, Cumbria, UK [40] was used to conduct γ radiation experiments. The maximum dose rate of 680 Gy/min can be provided by this γ radiation source [40]. However, the absorbed dose rate can be varied from 400 Gy/min to approximately 4 Gy/min using the distance from the source to the Device Under Test (DUT). It can be further reduced to 0.06 Gy/min with attenuation. These characteristics render the facility suitable for experimentation under a range of dose rates. Figure 1 illustrates the experimental setup employed in this research work.

The absorbed dose rates were measured using a Radcal Corporation Accu-Dose+ base unit equipped with a $10 \times 6-0.18$ ion chamber (S/N 47-0458). The absorbed dose rate was measured by placing the dose sensor right in front of the camera (in the irradiation cavity) and the measurement of the absorbed dose was carried out for a very small duration of gamma exposure (1 minute). This allows us to calculate the absorbed dose rate for the CMOS camera. The dose sensor was then removed from the cavity for the radiation experiment. The absorbed dose during the experiment can be easily calculated by multiplying the measured dose rate with the irradiation time.

The cavity at DCF is equipped with five lead attenuator blocks placed adjacent to each other in front of the source. Each block reduces the gamma flux by 2 times. The experiments related to the dark image analysis presented in Section IV are performed with all the attenuators in place. Dose rates were varied by changing the position of the cameras with in the cavity. For the images captured in presence of light source, the cameras were fixed to the cavity door and the chessboard image was pasted on the attenuator block. For these experiments, the dose rates were ramped up by removing the attenuator blocks while the cameras kept at fixed position as elucidated in Figure 2.

2) Test Samples: The sample used in this experiment is a Raspberry Pi Camera which is a low cost COTS CMOS image sensor. For each experiment, different Raspberry Pi cameras have been utilized to ensure reliability of the results. However, for the first half of the experiments, the cameras are covered with black tape to capture the dark images.

For the images caputured in presence of light source, a chessboard of 12×12 squares was used as an object of interest for the capture depicted in Figure 3. It was placed at a maximum distance (width of the cavity- 20 cm) from Raspberry Pi camera in the cavity. Chessboard images are used

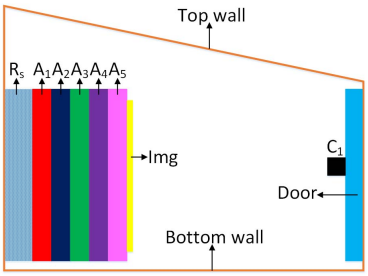

(a) $\dot{D}$ = 0.73 Gy/min

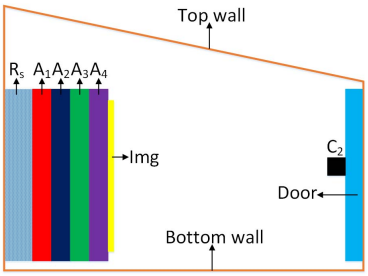

(b) $\dot{D}$ = 1.46 Gy/min

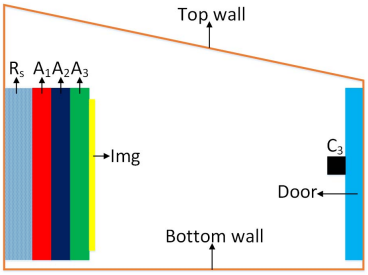

(c) $\dot{D}$ = 2.92 Gy/min

Fig. 2. Measurement setup for dose rate degradation analysis of chess board images where A_1, A_2, A_3, A_4, A_5 are the attenuation blocks (lead blocks), C_1, C_2, C_3 are the un-irradiated cameras utilized for the different dose rate experiment, R_S is the radiation source which consists of three cobalt rods, Img is the 12 × 12 chess board image.

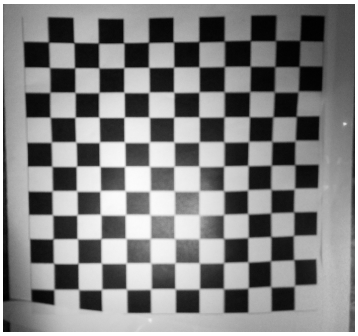

Fig. 3. Chessboard captured without any radiation.

widely for assessing image quality, calibrations of commercial cameras and mapping the target site [41]–[43].

The extension ribbon cable (2 m long) of the camera was used to place the camera control unit (Raspberry Pi board) outside the cavity to prevent it from being irradiated. During the experiment, the camera was accessed and controlled with software from within the Python programming language using the Pi Camera application programming interface (API). Raw-data format images were processed on the Raspberry Pi with a Python script utilizing the NumPy library and saved in the NumPy file format. The pre-processed raw images were later transferred to a separate computer and read into MATLAB with a NumPy data format reader. Further processing was accomplished using MATLAB. To the best of author's knowledge, we ensured that the images are captured without any pre-processing like "dark level correction", that takes place in the Image Signal Processor (ISP) of the Raspberry Pi's Graphical Processing Unit. Furthermore, a conscious effort has been made to disable the automatic gain control feature of the camera sensor while capturing the images by setting the camera exposure in 'off' mode (through Pi Camera) .

IV. Analysis of Dark Images

A. Evaluation Metrices

The characterization of the image sensor follows a standard procedure of measuring the sensor output in both complete dark and under illumination source. In our previous research [25], we had measured the dark response of three low cost CMOS cameras: 1) Raspberry Pi, 2) Trust USB Camera and 3) Spy Camera. The image degradation in the later two cameras Trust USB and Spy was more as compared to the Raspberry Pi camera. Therefore, in this work, we evaluate the image degradation of Raspberry Pi camera in detail in complete dark mode. To evaluate the degradation corresponding metrics for the dark condition has been described as follows.

1) Pixel Saturation Factor (PiSF): PiSF is the fraction of the sensor pixels that have pixel value greater than the threshold value (50% of the saturation value) and can be mathematically formulated as:

$$z = 0.5 \times saturation\ value$$
$$PiSF = \frac{number\ of\ pixel\ with\ value \geq z}{total\ number\ of\ pixels} \quad (1)$$

The reason behind selecting the specific threshold value of 50% is that (i) it coincides with the threshold value generally used for binarization of images [44], and (ii) It helps in evaluation of pixel charge induced by the radiations.

2) Gamma-Induced Photo Charge (DN) and Gamma-Induced Photo Signal (DN/S): Gamma-induced charge is the charge developed in the photosensitive device under dark conditions when the camera is exposed to gamma radiations. The source of this charge is the electrons released as a result of interaction of gamma radiations with silicon. The charge developed for a particular camera exposure time can be evaluated from the captured dark images using the following equation:

$$\mu_q = \frac{1}{LB} \sum_{l=0}^{L-1} \sum_{b=0}^{B-1} Img_q[l][b] \quad (2)$$

where, μ_q is the mean gamma induced charge, Img_q is the mean of η number of dark frames captured at a particular exposure time, and L×B is the resolution of the mean captured frame.

The amount of gamma-induced charge in the photosensitive device increases with the increase in the camera exposure/integration time. Therefore, an important metric is the rate

at which gamma induced charge increases with the increase in exposure time. This metric is termed as gamma-induced photo signal. The methodology to evaluate the mean gamma-induced signal is presented in Section IV-B.

The amount of charge induced in camera sensor for any arbitrary exposure time t_{exp} can be equated as:

$$\mu_q^{t_{exp}} = \mu_0 + \mu_s t_{exp} \tag{3}$$

where, μ_s is the mean gamma-induced signal, and μ_0 is the mean gamma-induced charge for zero exposure time. However, it is not possible to capture a frame with zero exposure time. Therefore, it is common to use the frame captured at the smallest possible exposure time to evaluate μ_0 (For our experiment minimum exposure time was 10 ms).

3) Photogenerated Noise (PN): PN is essentially the noise level during the irradiation in dark conditions. The source of this noise are the photo generated electron-hole pairs due to the exposure of camera to radiation. It can be calculated by evaluating the variance of temporal signal over a series of frames for individual pixel and then by taking the average of all the pixels, which identifies the noise over the image [45]:

$$\sigma^2_{y,dark} = \frac{1}{KN}\sum_{j=1}^{K}\sum_{i=1}^{N}(P_{ij} - M)^2 \tag{4}$$

$$PN = \sigma_{y,dark} \tag{5}$$

where K and N represent the total number of acquired frames and total number of pixels per frame, respectively. P_{ij} is the j^{th} pixel value from i^{th} frame and M is the mean value of all the j^{th} pixels of N frames.

4) Dynamic Range (DR): DR is the ratio of the pixel saturation level (μ_{sat}) and the noise floor (Photogenerated noise), as given by Equation 6.

$$Dynamic\ Range\ (dB) = 20\ log\ \frac{\mu_{sat}}{PN} \tag{6}$$

B. Evaluation Methodology

We capture a set of η number of frames under dark conditions[1] at different exposure times (varying between 10 ms and 1300 ms). This process is performed for images captured with and without radiation exposure. For each exposure time, we calculate a mean dark frame. This is followed by calculating parameters specified in Section IV-A using mean dark frame computed for each exposure rate. The parameters like PiSF, μ_q, DR, are computed using Equations 1, 3, 6, respectively. However, for gamma-induced photo signal, we compute the mean response $\frac{(Img_\zeta - Img_{\zeta'})}{(\delta t_{exp})}$. Img_ζ and $Img_{\zeta'}$ are the images captured at two different exposure times 10 ms and 1300 ms, respectively, and δt_{exp} is the difference between two exposure times, i.e. 1290 ms. The photogenerated noise is computed using Equation 5 utilizing the images captured at smallest integration time (10 ms).

Algorithm 1 elucidated the evaluation methodology used to evaluate the parameters of dark images. Five distinct dose rates (0.55 Gy/min, 1.34 Gy/min, 2 Gy/min, 3 Gy/min, and 4 Gy/min) experiments were performed to analyse the effect of gamma dose rate on the degradation of the mentioned metrics. For each dose rate experiment, a new un-irradiated camera was used to rule out any pre-experiment absorbed dose effect. The five different cameras (R1, R2, R3, R4, and R5) used in the experiments were all irradiated separately. For each dose rate experiment, dark images were captured (during irradiation) at the instant the cameras had been exposed to gamma dose of 100 Gy. Such scheduling ensures consistency of analysis as the metrics were evaluated using images captured from five different cameras irradiated to same dose of 100 Gy at five different dose rates.

[1]In our experimental setup, η is considered between 5 to 10.

Algorithm 1: Evaluation of Dark Images

Input:
1. $Img = \{Img_1, \ldots, Img_\eta\}$: Set of Dark Images;
2. χ : set of dose rate at which images are caputured;

Output: Evaluation metrices

for *each dose rate in* χ **do**
- Calculate mean dark frame for each exposure time
- **METRIC CALCULATION**
- Calculate PiSF,μ_q, DR using Equation 1, 3, 6;
- Calculate gamma-induced photo signal by computing mean response $\frac{(Img_\zeta - Img_{\zeta'})}{(\delta t_{exp})}$;
- Calculate the Photogenerated noise from Equation 5 using the images captured at smallest integration time (10 ms);

C. Results and Analysis

The evaluation of our metrics addresses four different directions: 1) Pixel distribution, 2) Gamma-induced photo charge, 3) Temporal variance and 4) Gamma-induced signal evolution with time. The results for each direction is discussed as follows.

1) Pixel Distribution: In this analysis, we look at the three evaluations 1) histogram distribution, 2) PiSF and 3) Dark Images. Figure 4 depicts the histogram distribution plot of the sensors' pixel values. The histogram distribution indicates the percentage of fractional pixel value with respect to the normalised pixel value. This representation facilitates the evaluation of the charge developed in the sensor after exposure to various levels of the gamma doses. A threshold of 50% of the saturation value is used to gauge the induced pixel charge. In normal condition, all sensor pixels have pixel value less than the threshold value. An instant image degradation is observed due to induction of gamma ray photo charge upon exposure of camera to the gamma radiations. The extent of induced charge depends on the gamma dose rate. For example, 8% of the pixels exceed the 50% saturation threshold at dose rate of 0.55 Gy/min. This number increases from 26% and 47% at dose rates of 1.34 Gy/min and 3 Gy/min, respectively. Furthermore, similar analysis can be performed for different threshold values.

Figure 5 shows PiSF plot as function of the gamma radiation dose rate. PiSF is a linear function of the dose rate with a

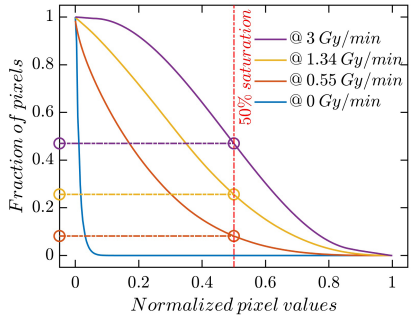

Fig. 4. Histogram distribution across different gamma dose rates (Absorbed dose=100 Gy, t_{exp} = 1300 ms).

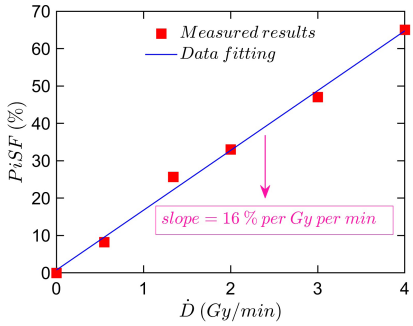

Fig. 5. PiSF v/s Dose Rate (Absorbed Dose = 100 Gy, t_{exp} = 1300 ms).

slope of 16% per Gy per min. It implies that all the image pixel values will exceed the threshold value if subjected to gamma radiation of dose rate greater than or equal to 6.25 Gy/min.

Figure 6 depicts the dark images captured by Raspberry Pi cameras when exposed to gamma radiation (for exposure time of 1300 ms). The cameras are irradiated to the same dose of 100 Gy, but at different dose rates. A gradual increase in the image pixels with very high gamma-induced charge is observed with increase in dose rate.

2) Gamma-Induced Photo Charge: The charge induced in the camera sensor under dark conditions when exposed to gamma radiation is known as gamma-induced photo charge. We analyse gamma-induced photo charge generated over the cross sectional area of our dark images. Figure 7 shows the gamma radiation-induced image degradation across the rows and columns of the dark images. A cross-section of 500 × 500 pixels from the centre of the image is selected for analysis. Figure 7(a) and Figure 7(b) depict the gamma-induced photo charge response of the central row and column vectors of the selected cross section for different dose rates. Furthermore, Figure 7(c) shows the gamma-induced photo charge of the row and the column vectors (at dose rate of 1.34 Gy/min) mapped on the same plot. Two observations evident from these plots are as follows:

1) The mean gamma-induced photo charge of the row and column vectors and its variation across the image pixels increases with increase in dose rate.
2) The gamma-induced charge variation across the column vector is more compared to row vector in the dark images as depicted in Figure 7(c).

Now, we analyse the image degradation by looking at the temporal variance in signal in form of PN.

3) Temporal Variance: In this section, we analyse the image degradation in light of three parameters related closely to temporal variance 1) PN, 2) Pixel saturation (μ_{sat}) and 3) DR. Figure 8(a) shows the PN of the sensor plotted for different dose rates. The PN increases with increase in the dose rate. The increase is observed to be approximately proportional to the square root of the dose rate. Figure 8(b) shows the normalized photogenerated noise (to pre-radiation value) of the sensor in log scale plotted for different dose rates. The noise floor is at 0 dB before exposure to gamma radiations. It increases with increase in the dose rate reaching approximately 25 dB at dose rate of 4 Gy/min. The increase in the noise floor plays a significant role in the degradation of parameter DR, that is analysed further in Figure 9.

Figure 9 depicts the effect of the gamma radiations on DR, PN and saturation output of the camera sensor when exposed to different gamma dose rates. The saturation output is the mean pixel saturation value represented in the log scale. The PN increases and the saturation output decreases with the gamma exposure as depicted in Figure 9. This eventually results in the reduction of the DR. Apart from an initial steep drop, the dynamic range reduces fairly linearly with the increase in the dose rate. The drop of 33.18 dB is observed in DR. DR is an important parameter of commercial cameras, particularly in context of producing high contrast images, as it represents the camera's ability to reliably produce the brightest and darkest portions of the image.

Though the analysis presented so far provide useful insight into the gamma-induced image degradation of the camera, there are several important aspects that need to be explored: (1) Evolution of the gamma-induced signal with time, and (2) Whether the gamma-induced signal is more sensitive to the radiation flux or the cumulative gamma dose? To explore these aspects, we analyse the evolution of gamma-induced signal in dark images with time.

4) Gamma-Induced Signal Evolution With Irradiation Time: The analysis so far mainly presents the effect of dose rate on the gamma-induced signal at a specific instant during the gamma irradiation. In this section, we analyse the evolution of the induced signal over the duration of the gamma irradiation with an intent to elucidate the difference between the gamma flux and absorbed cumulative dose effects. An experiment is performed to facilitate the said objective. A un-irradiated Raspberry Pi camera (R6) is exposed to a total dose of 250 Gy in five radiation cycles. Radiation cycles here refer to periods of constant dose rate gamma irradiation (of the same camera).

The dose rate during the first and fifth cycle is 2 Gy/min. The dose rate during the second and fourth cycle is 3 Gy/min. The dose rate during the third cycle is 4 Gy/min. The radiation exposure time duration during each cycle (25 mins for Cycle 1 and Cycle 5, 16.7 mins for Cycle 2 and Cycle 4, and 12.5 mins for Cycle 3) is set such that the camera receives the same dose of 50 Gy through out. The evaluation methodology discussed in Section IV-B is utilized to measure the gamma-induced signal at different points during the radiation cycles. Figure 10(a) shows the evolution of the induced signal over the

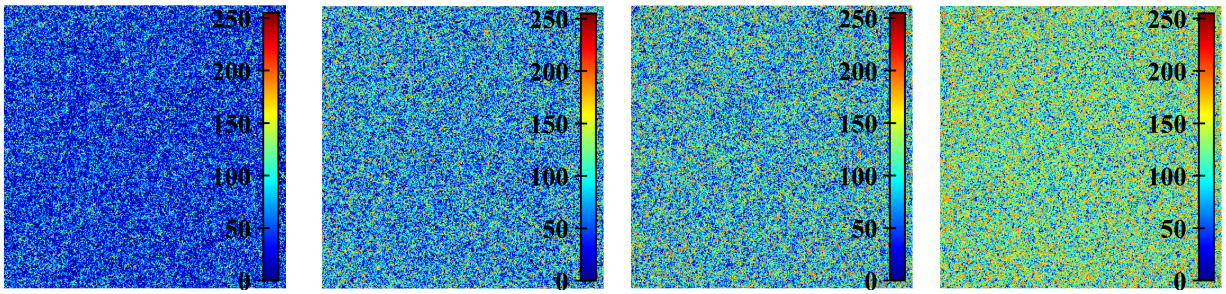

Fig. 6. Dark images captured using the Raspberry Pi cameras exposed to gamma irradiation (Absorbed dose=100 Gy, t_{exp} = 1300 ms) at dose rate of (a) 0.55 Gy/min (b) 1.34 Gy/min (c) 2 Gy/min (d) 4 Gy/min.

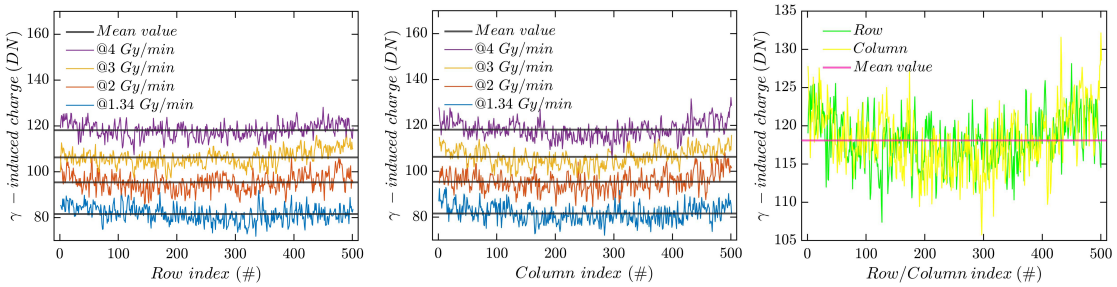

Fig. 7. Gamma-induced charge for dark images obtained at various dose rates of gamma radiation exposure (Absorbed dose=100 Gy, t_{exp} = 1300 ms) with respect to (a) row index (b) column index (c) row and column index.

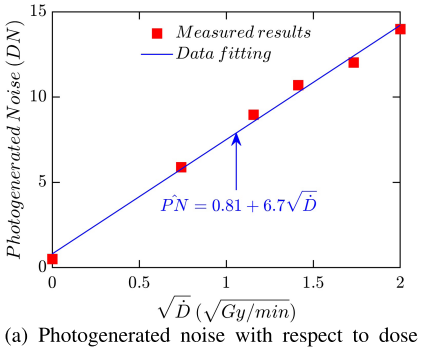

(a) Photogenerated noise with respect to dose rate

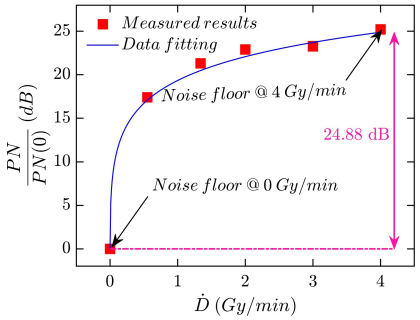

(b) Normalized photogenerated noise in log scale with respect to dose rate

Fig. 8. Photogenerated noise as function of dose rate during γ exposure (Absorbed dose=100 Gy, t_{exp} = 1300 ms).

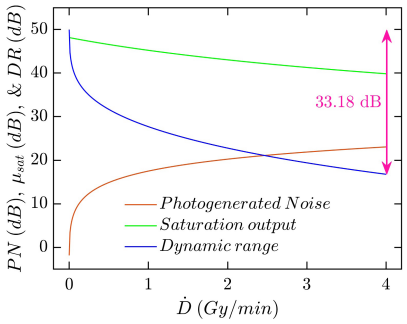

Fig. 9. Evaluation metrics variation for dark images at different gamma dose rates (Absorbed dose = 100 Gy, t_{exp} = 1300 ms).

radiation cycles. It is to be noted that there is a small window of 5 mins on the timeline at start of each cycle. This window represents the time when the radiation is off and setup is done for a dose rate measurement as discussed in Section III-A.

The following three important observations are noted from the Figure 10(a):

1) The gamma-induced signal appears to be more sensitive to the gamma photon flux as compared to cumulative radiation dose. This observation is consistent with earlier results reported in [16]. In this work, it was observed that the degradation of images captured during exposure of constant dose rate was more due to initial dose in comparison to the cumulative dose rate.
2) The induced signal in each cycle follows the pattern of the dose rate i.e. it increases from Cycle 1 to Cycle 3 and reduces in both the cycles, Cycle 4 and Cycle 5.
3) The mean induced signal is slightly higher in Cycle 5, as compared to Cycle 1 despite the fact that camera is exposed to the same gamma dose rate in both the

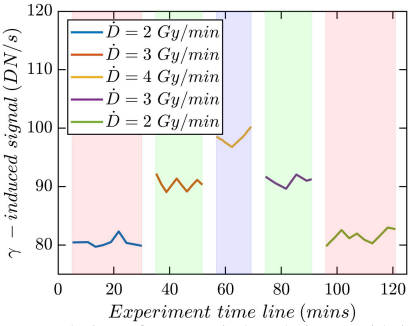

(a) Evolution of gamma-induced signal with irradiation time

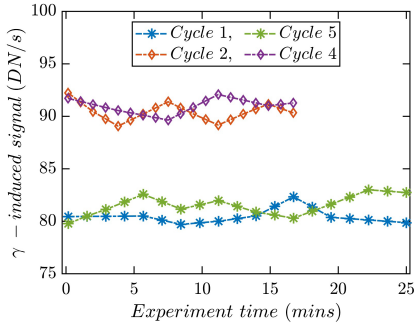

(b) Simultaneous mapping of induced signals in the same dose rate cycles during the gamma irradiation

Fig. 10. Evolution of gamma-induced signal during irradiation across the radiation cycles.

remaining cycles. The same is true for two cycles, Cycle 2 and Cycle 4, respectively.

The above mentioned observations are elucidated more clearly in Figure 10(b). The reason for this increase is the additional dose received by the camera between the Cycle 1 and Cycle 5 and Cycle 2 and Cycle 4.

V. Analysis of Images in Presence of Light Source

For our intended application of autonomous inspection of nuclear sites, the robot vision sensor (CMOS image sensor) will capture images in presence of illumination, most of the time image will have inhomogeneous illumination [46]. Therefore, after evaluating the images in dark conditions, we perform the analysis of image degradation in condition of light. For this analysis, we do not cover Raspberry Pi camera with the black tape and assess the quality of captured images. For each experiment at different dose rate, a new Raspberry Pi camera is used. The quality assessment is performed by analysing captured chessboard images.

A. Evaluation Metrics

While inspecting the nuclear site, robot intends to use images captured by CMOS image sensor for various purpose. We have identified two main purpose of captured images: 1) *surveillance*, 2) *navigation*. If the images captured are used for the purpose of survelliance, their image quality needs to be assessed. For the purpose of navigation, we need to asses if the radiated images can be used as an input for navigation by the robot. In order to pursue our aim of image quality analysis, we select standard metrics that resemble human visual system closely for evaluation. Since the field of view change for every dose rate, all the selected metrics are full reference images metrics, i.e., degradation quality of the radiated image is analysed in comparison to image without radiation exposure. The image without radiation exposure is known as a *'reference image'*, I_{ref}. Both, the reference image and radiated image have same field of view. The full-reference image quality metrics evaluated are described below.

1) Peak Signal to Noise Ratio (PSNR): PSNR is the ratio of maximum signal power to power of radiation noise. The signal refers to the reference image, I_{ref} and noise refers to the radiated image, I_r. It is calculated using mean squared error (MSE) which is defined as:

$$MSE = \frac{1}{LB}\sum_{i=0}^{l-1}\sum_{j=0}^{b-1}[I_{ref}[i][j] - I_r[i][j]]^2 \tag{7}$$

$$PSNR = 20log(I_{ref}) - 10log(MSE) \tag{8}$$

where I_{ref} has a resolution of size $L \times B$. Lower PSNR indicates higher radiation degradation. The parameter PSNR varies between ∞ to 0. So, the PSNR value for the non-irradiated camera (0 Gy/min) will be ∞. When the camera becames non-operational then the PSNR value will be 0.

2) Structural Similarity Index (SSIM): This metric aims to replicate human visual system which assess the quality of image based on its sensitivity to difference in structure. The quality of any image is assessed by comparing three components: *1) luminance (l), 2) contrast (c), and 3) structure (s)*. SSIM for a reference image I_{ref} and radiated image I_r is calculated as:

$$SSIM(I_{ref}, I_r) = [l(I_{ref}, I_r)]^{\alpha}[c(I_{ref}, I_r)]^{\beta}[s(I_{ref}, I_r)]^{\delta} \tag{9}$$

where α, β, δ are parameters which define relative importance of the three components. Higher the radiation degradation, lower is the SSIM value. The value of SSIM parameter varies between 0 and 1. The value of SSIM parameter for non-irradiated camera (0 Gy/min) will be 1. The SSIM parmeter will attain value 0 when the camera becames non-operational due to the absorbed dose.

3) Entropy: Entropy of any image indicates the statistical measure of randomness and is helpful in characterizing texture. An entropy of an image (I) can be defined as :

$$H(I) = \sum_{n=1}^{256} p_n(I)log_2(p_n(I)) \tag{10}$$

The entropy evaluation metric E for reference image I_{ref} and radiated image I_r can be defined as:

$$E(I_{ref}, I_r) = \frac{H(I_{ref})}{H(I_r)} \tag{11}$$

Higher the radiation induced noise in the images, higher is the entropy evaluation metric E value. The value of entropy value metric E varies between 1 and ∞. The value of metric E for non-irradiated camera (0 Gy/min) will be 1. The metric

will be ∞ when the camera becames non-operational due to absorbed dose.

4) Handcrafted Feature Matching Decline (HFMD): Handcrafted features are still deployed by robots as a fundamental method for visual odometry to estimate their locations. When the process of determining position and orientation of robot is carried out by analysing images, it is called as visual odometry [47]. In literature, many handcrafted feature-based methods have been proposed which extract features from images and match them with earlier images to estimates its position [48]. Features are set of interest points in images which are invariant to geometric and photometric changes such that even when the robot captures image from different viewpoints and illumination conditions the interest points are repeatable and can be easily matched from the original image. When the robots will be deployed in the nuclear site, the images captured by CMOS image sensors will have radaiation induced noise. Our aim is to evaluate how radiation noise affects the handcrafted features, for this purpose we use an evaluation metric which measures decline in matching of handcrafted features. Since, we have used a chessboard as an image of interest we use the popular Harris feature detectors [49] as an handcrafted feature detector. We use RANSAC [50] for outliers identification among the detected feature matches. The percentage of feature matching decline after radiation exposure is evaluated using following equation:

$$HFMD = \frac{M_{ref} - M_r}{M_{ref}} \tag{12}$$

where M_{ref} is the number of feature matches between a reference image with itself, and M_r is the number of features matches between the reference image and the radiated image. The value of $HFMD$ parameter varies between 0 and 1. The value of metric $HFMD$ for non-irradiated camera will be 0.

B. Evaluation Methodology

We capture a set of η number of frames under illumination source[2]. The chessboard of 12×12 is placed at end of the cavity (pasted on attenuator) such that field of view of the Raspberry Pi camera covers the entire chessboard. This is followed by calculating parameters specified in Section V-A using set of captured chessboard frames. Parameters like PSNR, SSIM and Entropy are computed using Equations 8, 9 and 11, respectively. However, to compute HFMD, first we detect Harris corner feature detector points $F = \{f_1, f_2, \ldots, f_m\}$ in both reference image and radiated image and match these detected points. Now, for a given distance, using the RANSAC methodology, we determine set of outliers. Finally, using Equation 12 we compute HFMD parameter. The experiments are performed at three distinct dose rates (0.73 Gy/min, 1.46 Gy/min, 2.92 Gy/min) to analyse the effect of gamma dose rate of images. For each experiment, a new un-irradiated camera was placed in the cavity to rule out any pre-experiment dose rate effect. The three different cameras (R7, R8 and R9) used in the experiments were all irradiated separately. Since, all the evaluation parameters required a reference image for calculation, a pre-radiated image was captured before each camera was exposed to radiation. The radiated image was captured after each camera had been exposed to 100 Gy.

As shown in Algorithm 1, we have calculated the above mentioned parameters for each distinct dose rate. In our experiment, the dose rates are varied between 0.0 Gy/min and 3 Gy/min.

Algorithm 2: Evaluation of Images in Presence of Light Source

Input:
1. $Img_r = \{Img_r^1, \ldots, Img_r^\eta\}$: Set of Images captured in presence of light ;
2. Img_{ref} : pre-radiated image;
3. χ : set of dose rate at which images are caputured;

Output: Evaluation metrices

```
for each dose rate in χ do
    METRIC CALCULATION
    Calculate PSNR, SSIM, Entropy using
     Equation 8, 9, 11;
    Determine Harris feature points for reference image
     F_{Img_ref} and radiated image F_{Img_r}.
    Match the harris points in reference image with
     radiated image. Remove the outliers in the matches
     using RANSAC.
    Calculate the HFMD parameter using Equation 12;
```

C. Results and Analysis

The evaluation of our metrics for images captured in presence of light source can be characterised in two categories: 1) Image Quality Analysis (IQA) and 2) Handcrafted Feature Analysis (HFA). The results obtained for each category are discussed in detail in the following sub-sections.

1) IQA: In the first category, the main aim is to analyse the image quality of radiated images for the purpose of surveillance. Since, the field of view and illumination condition change at every dose rate, we look at three full reference metrics 1) PSNR, 2) SSIM and 3) Entropy. Since, all three IQA metrics are full reference, this implies that to compute these three metrics we need two images: 1) Reference Image (I_{ref}) captured when image sensor is not subjected to any radiation and 2) Radiated Images (I_r) when the image sensor is subjected to gamma radiation at certain dose rate. Both the images I_{ref} and I_r are captured in the same environmental settings. Images obtained with and without γ radiation of dose rate 2.92 Gy/min are illustrated in Figure 11.

Figure 12(a) depicts the PSNR with respect to varying dose rate. This representation facilitates evaluation of image quality in terms of corrupting radiation induced noise. Higher values are indicative of better quality of image. The PSNR value across varying dose rate is indicative of the fact that PSNR value decreases with increase in dose rate. This implies that, as the dose rate increases, the radiation induced noise also increases. Similarly, we analyse the SSIM parameter with respect to dose rate. Figure 12(b) illustrates that SSIM

[2]In our experimental setup, η is considered between 5 to 10.

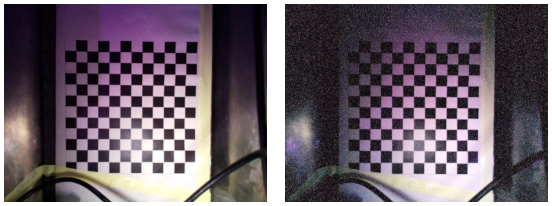

(a) (b)

Fig. 11. Chessboard images obtained with and without γ radiation (Absorbed dose = 100 Gy, t_{exp} = 1300 ms) (a) Pre-radiated image captured before camera is exposed to 2.92 Gy/min (b) Radiated image when camera is exposed to 2.92 Gy/min.

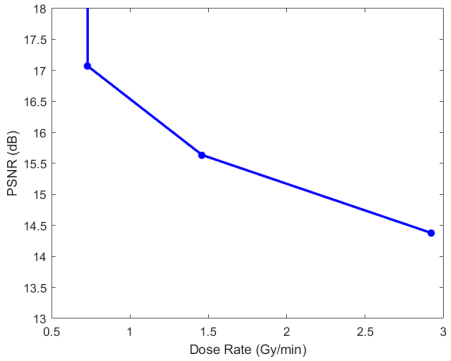

(a) PSNR with respect to dose rate

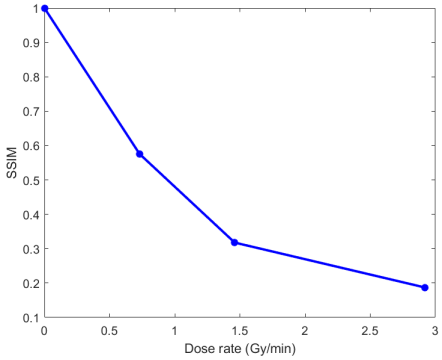

(b) SSIM with respect to dose rate

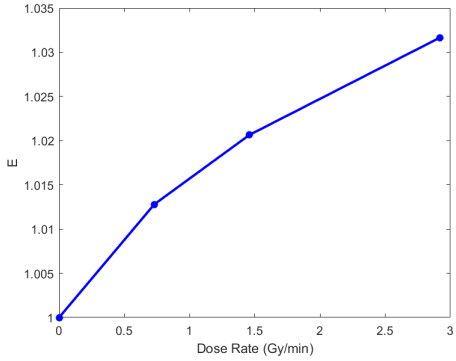

(c) Entropy with respect to dose rate

Fig. 12. IQA metric with respect to varying γ radiation dose rate(Absorbed dose = 100 Gy, t_{exp} = 1300 ms).

decreases with increase in dose rate. Higher SSIM parameter is indicative of less noise. This reinforces our previous observation that if the sensor is exposed to higher dose rate, the image captured has higher induced radiation noise.

To establish this further, we evaluate the image quality at different dose rate using entropy. Entropy is a statistical measure of randomness. Lesser value of entropy metric E is indicative of better quality of image. Figure 12(c) shows that as the dose rate increases, the entropy metric E increases. This elucidates that with the increment in dose rate the image quality decreases indicating that higher dose rate exposure results in the decline of image quality. However, the CMOS image sensor was operational for all the dose rates with absorbed dose of 100 Gy. Previous studies [16] have found CMOS image sensor to be operational till the absorbed dose of 1549 Gy when radiated with a constant dose rate of 0.5 Gy/min. The radiated images are found useful for the purpose of surveillance till absorbed dose rate of 500 Gy. To gauge the usefulness of the image, the image quality was quantified using parameter PSNR and SSIM which were measured as 4.7 dB and 0.2, respectively. In our experiment for different dose rates, the value of PSNR parameter varies between 17.0711 dB - 14.3798 dB. The value of SSIM parameter varies between 0.5756 - 0.1872. Entropy however, has not been used in literature as parameter to measure degradation due to gamma rays but fast neutron [9]. Entropy was a good measure of degradation in case of fast neutron as the radiation noise appeared in form of temporal blobs increasing the randomness in image. In the experiment, we found out that the entropy evaulation metric E varied between 1.0128 - 1.0317, not showing a substantial variation as the image degradation increased with increase in the dose rate. From the evaulation of all the three image quality parameters, we can conclude that for the dose rates relevant for inspection of nuclear site, the images captured by the robot using CMOS image sensor for surveillance purpose are useable.

After evaluating IQA metric, we evaluate whether images can be used as visual input for navigation by analysing HFA parameter.

2) HFA: Handcrafted features play an important role in visual odometry, allowing robot to estimate its location. In this section, we analyse the effect of radiation in terms of matches of handcrafted features in the images captured when the sensor is exposed to γ radiation. Since, the object of interest captured is a chessboard, we use Harris feature detector to identify feature points in the image captured. As evident from Figure 13(a), the detected Harris feature points in the image consist of corner points in the chessboard images along with feature points in the wires placed in the background.

We perform similar operations using detected Harris feature points for radiated images. Figure 13(b) shows Harris feature points for image captured when the sensor is exposed to γ radiation of 2.92 Gy/min. We observe from Figure 13 that the radiation induces salt and pepper noise in images degrading the quality. This proves to be adversarial for Harris feature detection to identify feature points in the images. For the robot to estimate its position, the Harris features detected in the reference images should be repeatable in the radiated image. However, due to radiation noise instead of identifying the corners of chessboard as features, the radiation noise is identified as Harris feature.

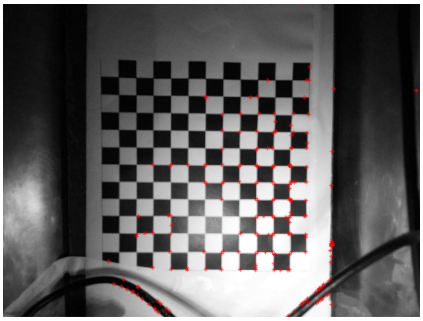

(a) Pre-radiated image with Harris feature points

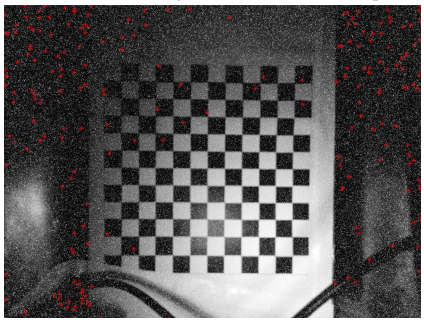

(b) Harris feature points in image radiated at dose rate 2.92 Gy/min

Fig. 13. Harris feature points detected for images obtained with and without gamma radiation.

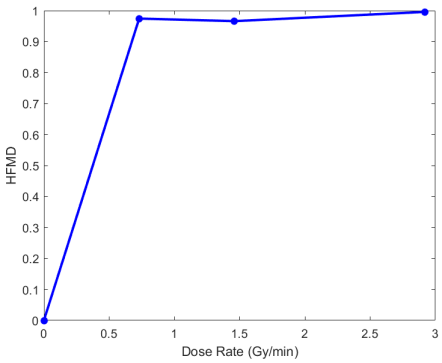

Fig. 14. HFMD with respect to varying γ radiation dose rate (Absorbed dose $= 100$ Gy, $t_{exp} = 1300$ ms).

After detecting Harris feature points in both reference images and radiated images, we match the features detected in both the images. The outliers in the feature matches are eliminated using RANSAC algorithm. Finally, we analyse Harris feature points matching decline in terms of evaluation metric 'HFMD' calculated using Equation 12. Figure 14 depicts the variation of HFMD with respect to dose rate. We observe that HFDM parameter varies between 0.9744-0.9959 for the dose rate varying between 0 to 3 Gy/min. To the best of author's knowledge, no such work targeting analysis of feature matching decline due to gamma radiation has been done. But, the parameter of feature matching decline has been used for the matching images with perturbation [51]. However, it was pointed out in [51] that if the feature matching parameter decline by 92.37% the loop closure using Harris feature in SLAM (ability of robot to recognize previously visited place) fails completely. This allowed us to conclude that the radiated images cannot be used as an input for the purpose of visual odometry.

VI. Conclusion and Future Work

This study investigates the gamma-induced image degradation in the Raspberry Pi camera, a robot vision sensor, for dose levels realistic for the inspection of non critical areas of nuclear site environment. However, similar total ionizing dose levels (100Gy - 1kGy) can be found in medical and space applications [52]. The inaccurate sensing due to the absorbed dose rate present significant challenges to robot's long term autonomy in gamma radiation field. Our previous studies had elucidated that Raspberry Pi camera was able to perform better than its counterpart COTS robot vision sensors. The less image degradation is observed in CMOS image sensor with smaller pixel sensitive volume which is responsible for reduction in gamma-induced photo signal. This finding motivated us to further analyse the degradation of Raspberry Pi camera under various evaluation metrics.

The relevant evaluation metrics were calculated first for dark images captured at different dose rates. The evaluation metrics could be categorised in four classes: 1) Pixel Distribution, 2) Gamma-induced photo signal, 3) Temporal Variance and 4) Gamma-induced signal evolution with irradiation time. After evaluating the dark images, we computed the degradation in images captured when Raspberry Pi is exposed to light source. To make the experiment more realistic, we captured the image of chessboard as it is used by robot as an object for calibration and other visual odometric operations. There were two main objectives of analysing the degradation of images captured in light source. The first aim was to gauge the image quality for surveillance purpose and second aim was to assess whether radiated images can be used for the purpose of visual odometry. The image degradation analysis was classified in two classes: 1) Image quality and 2) Handcrafted features. The two diagnosis methodologies to evaluate the radiation induced image degradation allowed us to conclude that when the sensor is exposed to radiation upto 3 Gy/min, the images can be used for surveillance purpose. However, with the decline in HFMD parameter, radiated images cannot be used for visual odometry as handcrafted features are no longer repeatable. These parameters are indicative of faulty localisation, allowing the robot control system to know when to stop trusting the images captured by robot vision sensor based on radiometric reading.

This evaluation can allow generation of future mitigation strategies such as radiation noise removal which will allow adjustment of the images captured by robot according to a pre-programmed pattern. Based on the observations of the experiments carried out in this paper, it will be worthwhile to explore the following aspects in the future radiation experiments.

1) The analysis of the dark images captured during the radiation cycles provides insights into the radiation-induced signal and noise. However, these effects are not permanent and are observed only during the duration of the radiation cycles. The dark images may be captured between the radiation cycles in the future experiment.

The analysis of these images will provide insights into the parameters more relevant to sensor health such as dark charge, dark current, and read noise.

2) The sensor parameters listed above may be measured for different absorbed doses. The evaluation of healing of these parameters with time and post radiation cycles may be conducted for different cumulative doses.
3) Finally, the temperature of the camera sensor may be monitored over the duration of the experiment as it can effect both the radiation-induced signal and the dark current. However, the monitoring of temperature during the radiation cycle will be cumbersome as the reliability of the temperature sensor may be compromised due to the exposure to gamma radiations.

These findings will be useful in understanding vulnerabilities and failure points of other CMOS image sensors which have similar operating system and supporting signal processing electronics.

ACKNOWLEDGMENT

The authors acknowledge the support of The University of Manchester's Dalton Cumbrian Facility (DCF), a partner in the National Nuclear User Facility, the EPSRC U.K. National Ion Beam Centre, and the Henry Royce Institute. They also recognize Dr. Ruth Edge for her assistance during the radiation experiment.

REFERENCES

[1] T. Kotthauser and G. F. Mauer, "Vision-based autonomous robot control for pick and place operations," in *Proc. IEEE/ASME Int. Conf. Adv. Intell. Mechatronics*, Jul. 2009, pp. 1851–1855.
[2] S. Kawatsuma, M. Fukushima, and T. Okada, "Emergency response by robots to fukushima-daiichi accident: Summary and lessons learned," *Ind. Robot, Int. J.*, vol. 39, no. 5, pp. 428–435, Aug. 2012.
[3] B. Bird *et al.*, "A robot to monitor nuclear facilities: Using autonomous radiation-monitoring assistance to reduce risk and cost," *IEEE Robot. Autom. Mag.*, vol. 26, no. 1, pp. 35–43, Mar. 2019.
[4] T. A. Ferguson and L. Lu, "Fault tree analysis for an inspection robot in a nuclear power plant," *IOP Conf. Ser., Mater. Sci. Eng.*, vol. 235, Sep. 2017, Art. no. 012003.
[5] D. M. Fleetwood, "Total ionizing dose effects in MOS and low-dose-rate-sensitive linear-bipolar devices," *IEEE Trans. Nucl. Sci.*, vol. 60, no. 3, pp. 1706–1730, Jun. 2013.
[6] J. R. Schwank, "Total dose effects in MOS devices," in *Proc. IEEE NSREC Short Course*, Jul. 2002, vol. 111, no. 123, pp. 1–123.
[7] H. L. Hughes and J. M. Benedetto, "Radiation effects and hardening of MOS technology: Devices and circuits," *IEEE Trans. Nucl. Sci.*, vol. 50, no. 3, pp. 500–521, Jun. 2003.
[8] B. Aslam, "Measuring the degradation of commercial cameras under fast neutron beam," in *Proc. 28th Annu. Single Event Effects (SEE) Symp. Mil. Aerosp. Program. Log. Devices (MAPLD) Workshop*, 2019, pp. 1–16.
[9] Z. Khanam *et al.*, "Degradation measurement of Kinect sensor under fast neutron beamline," in *Proc. IEEE Radiat. Effects Data Workshop*, Jul. 2019, pp. 1–5.
[10] Z. J. Diggins *et al.*, "Range-finding sensor degradation in gamma radiation environments," *IEEE Sensors J.*, vol. 15, no. 3, pp. 1864–1871, Mar. 2015.
[11] K. E. Holbert, S. Sankaranarayanan, and S. S. McCready, "Response of lead metaniobate acoustic emission sensors to gamma irradiation," *IEEE Trans. Nucl. Sci.*, vol. 52, no. 6, pp. 2583–2590, Dec. 2005.
[12] V. Goiffon *et al.*, "Radiation hardening of digital color CMOS camera-on-a-chip building blocks for multi-MGy total ionizing dose environments," *IEEE Trans. Nucl. Sci.*, vol. 64, no. 1, pp. 45–53, Jan. 2017.
[13] J. W. Cho, Y. S. Choi, and K. M. Jeong, "Monitoring performance of the cameras under the high dose-rate gamma ray environments," *Health Phys.*, vol. 106, pp. S47–S58, May 2014.
[14] G. R. Hopkinson, M. D. Skipper, and B. Taylor, "A radiation tolerant video camera for high total dose environments," in *Proc. IEEE Radiat. Effects Data Workshop*, Jul. 2002, pp. 18–23.
[15] C. Wang, S. Hu, C. Gao, and C. Feng, "Nuclear radiation degradation study on HD camera based on CMOS image sensor at different dose rates," *Sensors*, vol. 18, no. 2, p. 514, Feb. 2018.
[16] J. Fagerström, "Ionizing radiation effects on image sensors: Method on evaluation from an image quality perspective," Dept. Elect. Inf. Technol., Lund Univ., Lund, Sweden, Tech. Rep. 8877372, 2016.
[17] Z. Wang *et al.*, "Characterization of total ionizing dose damage in COTS pinned photodiode CMOS image sensors," *AIP Adv.*, vol. 6, no. 3, Mar. 2016, Art. no. 035205.
[18] Z. Wang *et al.*, "Fixed pattern noise and temporal noise degradation induced by radiation effects in pinned photodiode CMOS image sensors," *IEEE Trans. Nucl. Sci.*, vol. 65, no. 6, pp. 1264–1270, Jun. 2018.
[19] X. Meng, K. D. Stefanov, and A. D. Holland, "Proton and gamma radiation effects on a fully depleted pinned photodiode CMOS image sensor," *IEEE Trans. Nucl. Sci.*, vol. 67, no. 6, pp. 1107–1113, Jun. 2020.
[20] X. Shoulong, Z. Shuliang, and H. Youjun, "γ-ray detection using commercial off-the-shelf CMOS and CCD image sensors," *IEEE Sensors J.*, vol. 17, no. 20, pp. 6599–6604, Oct. 2017.
[21] M. Pérez *et al.*, "Particle detection and classification using commercial off the shelf CMOS image sensors," *Nucl. Instrum. Methods Phys. Res. A, Accel. Spectrom. Detect. Assoc. Equip.*, vol. 827, pp. 171–180, Aug. 2016.
[22] V. Goiffon *et al.*, "Radiation effects in pinned photodiode CMOS image sensors: Pixel performance degradation due to total ionizing dose," *IEEE Trans. Nucl. Sci.*, vol. 59, no. 6, pp. 2878–2887, Dec. 2012.
[23] C. Virmontois *et al.*, "Radiation effects in pinned photodiode CMOS image sensors: Variation of epitaxial layer thickness," *IEEE Trans. Nucl. Sci.*, vol. 64, no. 1, pp. 38–44, Jan. 2017.
[24] I. Tsitsimpelis, C. J. Taylor, B. Lennox, and M. J. Joyce, "A review of ground-based robotic systems for the characterization of nuclear environments," *Prog. Nucl. Energy*, vol. 111, pp. 109–124, Mar. 2019.
[25] B. Aslam *et al.*, "Gamma-induced degradation analysis of commercial off-the-shelf camera sensors," in *Proc. IEEE Sensors*, Oct. 2019, pp. 1–4.
[26] *Raspberry Pi Camera*. Accessed: Nov. 7, 2020. [Online]. Available: https://www.raspberrypi.org/products/camera-module-v2
[27] *Spy Camera*. Accessed: Nov. 7, 2020. [Online]. Available: https://www.eyetek.co.uk/product-category/wireless-spy-cameras
[28] *Trust USB Camera*. Accessed: Nov. 7, 2020. [Online]. Available: https://www.trust.com/en/trust/webcam
[29] J. K. C. Leung, "Application of shielding factors for protection against gamma radiations during a nuclear accident," *IEEE Trans. Nucl. Sci.*, vol. 39, no. 5, pp. 1512–1518, Oct. 1992.
[30] Government of Japan. (Jun. 2011). *Report of Japanese Government to the IAEA Ministerial Conference on Nuclear Safety: The Accident at TEPCO's Fukushima Nuclear Power Station*. [Online]. Available: http://japan.kantei.go.jp/kan/topics/201106/iaea_*houkokusho*_e.html
[31] D. Klein and M. Corradini, "FUKUSHIMA DAIICHI: ANS committee report," ANS, La Grange Park, IL, USA, Tech. Rep. 71150, Jun. 2012. [Online]. Available: http://fukushima.ans.org/report/Fukushima_report.pdf
[32] P. C. Bennett and L. D. Posey, "RHOBOT: Radiation hardened robotics," Sandia National Labs., Albuquerque, NM, USA, Tech. Rep. Sandia Rep. SAND-97-2405, Oct. 1997.
[33] Q. Zhang *et al.*, "Research progress of nuclear emergency response robot," *IOP Conf. Ser., Mater. Sci. Eng.*, vol. 452, Dec. 2018, Art. no. 042102.
[34] C. Ducros *et al.*, "RICA: A tracked robot for sampling and radiological characterization in the nuclear field," *J. Field Robot.*, vol. 34, no. 3, pp. 583–599, May 2017.
[35] M. Zavala, "Autonomous detection and characterization of nuclear materials using co-robots," Ph.D. dissertation, School Mech. Eng., Georgia Inst. Technol., Atlanta, GA, USA, 2016.
[36] K. Nagatani *et al.*, "Emergency response to the nuclear accident at the fukushima daiichi nuclear power plants using mobile rescue robots," *J. Field Robot.*, vol. 30, no. 1, pp. 44–63, Jan. 2013.
[37] *Highest Radiation Reading Since 3_11 Detected at Fukushima No. 1 Reactor*. Accessed: Nov. 7, 2020. [Online]. Available: https://www.japantimes.co.jp/news/2017/02/03/national/fukushima-radiation-level-highest-since-march-11/XRiy_I-xWUk
[38] *Radiation Levels Now*. Accessed: Nov. 7, 2020. [Online]. Available: http://www.chernobylgallery.com/chernobyl-disaster/radiation-levels/

[39] B. Medvedev, "JPRS report: Soviet Union economic affairs chernobyl notebook," USSR Acad. Sci., Moscow, Russia, Tech. Rep. 18220199, Jun. 1989.
[40] *Dalton Cumbrian Facility*. Accessed: Nov. 7, 2020. [Online]. Available: http://www.dalton.manchester.ac.uk/recycle-bin/daltoncumbrianfacility/discover/facilities/co-60irradiator
[41] D.-X. Zhu, "Binocular vision-SLAM using improved SIFT algorithm," in *Proc. 2nd Int. Workshop Intell. Syst. Appl.*, May 2010, pp. 1–4.
[42] H. Wang, J. Pi, T. Qin, S. Shen, and B. E. Shi, "SLAM-based localization of 3D gaze using a mobile eye tracker," in *Proc. ACM Symp. Eye Tracking Res. Appl.*, Jun. 2018, pp. 1–5.
[43] B. Li, L. Heng, K. Koser, and M. Pollefeys, "A multiple-camera system calibration toolbox using a feature descriptor-based calibration pattern," in *Proc. IEEE/RSJ Int. Conf. Intell. Robots Syst.*, Nov. 2013, pp. 1301–1307.
[44] A. Shrivastava, and D. K. Srivastava, "A review on pixel-based binarization of gray images," in *Proceedings of the International Congress on Information and Communication Technology*. Singapore: Springer, 2016.
[45] *Standard for Characterization of Image Sensors and Cameras*, Standard EMVA Standard 1288, Release 3.0, Release European Machine Vision Association, 2010.
[46] K. H. Shin and Y. H. Lee, "An ergonomic evaluation of the illumination level and the management plan to improve the working environment of nuclear power plants," in *Proc. Trans. Korean Nucl. Soc. Fall Meeting*, Oct. 2011, pp. 1–2.
[47] D. Scaramuzza and F. Fraundorfer, "Visual odometry [tutorial]," *IEEE Robot. Autom. Mag.*, vol. 18, no. 4, pp. 80–92, Dec. 2011.
[48] H. Badino, A. Yamamoto, and T. Kanade, "Visual odometry by multi-frame feature integration," in *Proc. IEEE Int. Conf. Comput. Vis. Workshops*, Dec. 2013, pp. 222–229.
[49] L. Gueguen and M. Pesaresi, "Multi scale harris corner detector based on differential morphological decomposition," *Pattern Recognit. Lett.*, vol. 32, no. 14, pp. 1714–1719, Oct. 2011.
[50] O. Chum and J. Matas, "Optimal randomized RANSAC," *IEEE Trans. Pattern Anal. Mach. Intell.*, vol. 30, no. 8, pp. 1472–1482, Aug. 2008.
[51] Z. Ali, M. L. Anjum, and W. Hussain, "Adversarial examples for handcrafted features," in *Proc. BMVC*, 2019, pp. 1–14.
[52] V. Goiffon, "Radiation effects on CMOS active pixel image sensors," Institut Supérieur de l'Aéronautique et de l'Espace (ISAE-SUPAERO), Univ. de Toulouse, Toulouse, France, Tech. Rep. 14554, 2015, pp. 295–332.

Zeba Khanam received the B.Tech. degree in computer engineering from Aligarh Muslim University, Aligarh, India, in 2013, where she was awarded a gold medal for securing first rank, and the M.Tech. degree in advanced electronic systems from the Academy of Scientific and Innovative Research, India, in 2015. She is currently pursuing the Ph.D. degree with the University of Essex. She has worked as a Scientist with the Machine Vision Laboratory, CSIR-CEERI, India, which allowed her to gain industrial and academic experience in computer vision and embedded systems application in minimally invasive surgery and endoscopy. She is a Research Officer with the Embedded and Intelligent Systems Laboratory, University of Essex. Her current research interests include robot vision and path planning in nuclear environment.

Bilal Aslam received the B.Sc. degree in electrical engineering from the University of Engineering and Technology (UET) Taxila, Pakistan, in 2007, the M.S. degree in electrical engineering from the National University of Science and Technology (NUST) in 2013, and the Ph.D. degree in telecommunication engineering from UET Taxila in 2017. From March 2018 to January 2020, he worked as a Senior Research Officer with the Embedded Intelligent Systems (EIS) Laboratory, University of Essex, Colchester, U.K. He is currently working as an Assistant Professor with the Department of Electronics Engineering, UET Taxila. His research interests include RFID tag antennas, RF-based sensors, and measuring and modeling radiation-induced degradation of commercial vision sensors.

Sangeet Saha received the B.Tech. degree in information technology, the M.Tech. degree in computer science and engineering, and the Ph.D. degree from the University of Calcutta, Kolkata, in 2011, 2013, and 2018, respectively. In 2018, he was a Research Fellow with Tata Consultancy Services (TCS). He has been appointed as a Senior Research Officer with the Embedded and Intelligent Systems (EIS) Research Group, University of Essex, Colchester, U.K., since May 2018. His current research interests include real-time scheduling, scheduling for reconfigurable computers, real-time and fault-tolerant embedded systems, and cloud computing.

Xiaojun Zhai (Member, IEEE) received the Ph.D. degree from the University of Hertfordshire, U.K., in 2013. He is currently a Lecturer with the Embedded Intelligent Systems Laboratory, University of Essex. He has authored/coauthored over 60 scientific article in international journals and conference proceedings. His research interests include design and implementation of the digital image and signal processing algorithms, custom computing using FPGAs, embedded systems, and hardware/software co-design. He is a member of BCS and a Fellow of HEA.

Shoaib Ehsan (Senior Member, IEEE) received the B.Sc. degree in electrical engineering from the University of Engineering and Technology, Taxila, Pakistan, in 2003, and the Ph.D. degree in computing and electronic systems (with specialization in computer vision) from the University of Essex, Colchester, U.K., in 2012. He has an extensive industrial and academic experience in the areas of embedded systems, embedded software design, computer vision, and image processing. His current research interests include intrusion detection for embedded systems, local feature detection and description techniques, and image feature matching and performance analysis of vision systems. He was a recipient of the University of Essex Post Graduate Research Scholarship, the Overseas Research Student Scholarship, and the prestigious Sullivan Doctoral Thesis Prize awarded annually by the British Machine Vision Association.

Rustam Stolkin (Member, IEEE) received the M.Eng. degree in engineering science from the University of Oxford, Oxford, U.K., in 1998, and the Ph.D. degree in computer vision from University College London, London, U.K., in 2004. He is currently the Director and the Royal Society Industry Fellow of the National Centre for Nuclear Robotics, Birmingham, U.K., and a Professor of Robotics with the University of Birmingham, Birmingham, where he is the Founder and the Director of the Extreme Robotics Laboratory. He is also the Director of Spinout Company A.R.M. Robotics Ltd., Spain. He is highly interdisciplinary, with research interests spanning computer vision and image processing, machine learning and AI, robotic grasping and manipulation, and human–robot interaction.

Klaus McDonald-Maier (Senior Member, IEEE) is currently the Head of the Embedded and Intelligent Systems Laboratory, University of Essex, Colchester, U.K. He is also the Chief Scientist with UltraSoC Technologies Ltd., the CEO of Metrarc Ltd., and a Visiting Professor with the University of Kent. His current research interests include embedded systems and system-on-chip design, security, development support and technology, parallel and energy-efficient architectures, computer vision, data analytics, and the application of soft computing and image processing techniques for real-world problems. He is a member of VDE and a Fellow of the IET.